ACS APPLIED MATERIALS & INTERFACES

Research Article

www.acsami.org

Thermal Diffusivity of Hexagonal Boron Nitride Composites Based on Cross-Linked Liquid Crystalline Polyimides

Yu Shoji,[†] Tomoya Higashihara,[†,‡] Masatoshi Tokita,[†] Junko Morikawa,[†] Junji Watanabe,[†] and Mitsuru Ueda*[,†]

[†]Department of Organic and Polymeric Materials, Graduate School of Science and Engineering, Tokyo Institute of Technology, 2-12-1 H-120, O-okayama, Meguro-Ku, Tokyo 152-8550, Japan

[‡]PRESTO, Japan Science and Technology Agency (JST), 4-1-8, Honcho, Kawaguchi, Saitama 332-0012, Japan

Supporting Information

ABSTRACT: Hexagonal boron nitride (h-BN) composites with the oriented cross-linked liquid crystalline (LC) polyimide have been developed as high thermally conductive materials. Well-dispersed h-BN composite films were obtained, as observed by scanning electron microscopy. The morphology of the composite films was further investigated in detail by the wide-angle X-ray diffraction. The obtained composite films based on the cross-linked LC polyimide showed that the polymer chains vertically aligned in the direction parallel to the films, while those based on the amorphous polyimide showed an isotropic nature. Moreover, the alignment of the cross-linked LC polyimides was maintained, even after increasing the volume fraction of h-BN. This alignment plays an important role in the effective phonon conduction between h-BN and the matrices. Indeed, the thermal diffusivity in the thickness direction of the composite films based on the LC polyimide measured by a temperature wave analysis method was increased to 0.679 $mm^2 s^{-1}$ at a 30 vol % h-BN loading, which was higher than that based on the amorphous polyimide.

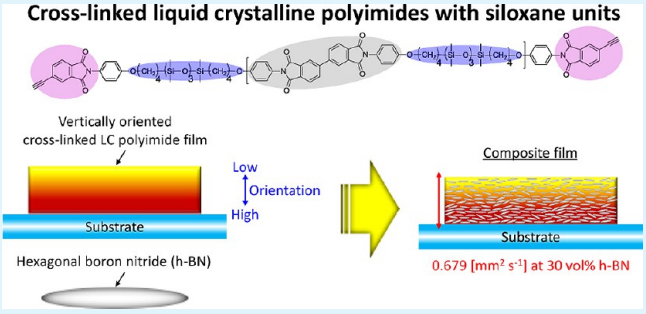

KEYWORDS: *liquid crystalline polyimide, cross-link, siloxane unit, hexagonal boron nitride, composite, thermal diffusivity*

INTRODUCTION

Toward integration, miniaturization, and functionalization of electronics, the development of high-density packing technologies is currently accelerated. However, the accumulation of heat generated inside the devices becomes problematic during the device operation because the insulating layers, such as the polymeric materials, between the semiconductors generally act as thermal insulators. Therefore, high thermally conductive insulating materials have recently been attractive materials for releasing the generated heat from the devices to produce further integrated circuits. Indeed, the polymeric materials have quite low thermal conductivities, usually from 1 to 3 orders lower than those of the ceramics and metals.[1] There is an approach to improve the thermal conductivity of polymeric materials through the addition of high thermally conductive fillers such as carbon materials[2−9] and ceramics.[10−18] However, a large amount of fillers leads to reducing the processability of those, increasing the melt or solution viscosity. In addition, the adhesion ability between the composite materials and the substrates becomes poor because of the high roughness of the material surface with the increasing ratio of fillers. Hence, decreasing the amount of the fillers is important to maintain such processing properties without sacrificing thermal conductivity. For instance, Hsu et al.[15] reported that the polymeric composites consisting of micro- and nanosized hybrid boron nitride (m- and n-BN) particles achieved a high thermal conductivity of 1.2 W m^{-1} K^{-1} at a relatively low weight fraction of 30 wt % BN loading in the case of the 7/3 weight fraction of m-BN/n-BN, which forms a random conductive bridge or network. However, the thermal conductivity of the single hexagonal BN (h-BN) composites is still low, which is less than 0.5 W m^{-1} K^{-1} at 30 wt % (ca. 20 vol %) h-BN loading. There are many established models for the composite systems to predict thermal conductivity.[2,19] According to the Bruggeman theoretical model,[19] the high thermally conductive composites with a small amount of fillers can be produced by increasing the thermal conductivity of the polymer matrices 2 or 3 times that of the conventional polymers. Therefore, the development of the high thermally conductive polymers is an effective approach to achieve the production of high thermally conductive composites containing a small amount of the fillers (<60 vol %). To increase the thermal conductivity of the organic polymers, controlling the orientation of the polymer chains is an effective way to efficiently conduct a "phonon",

Received: February 3, 2013
Accepted: March 18, 2013
Published: March 18, 2013

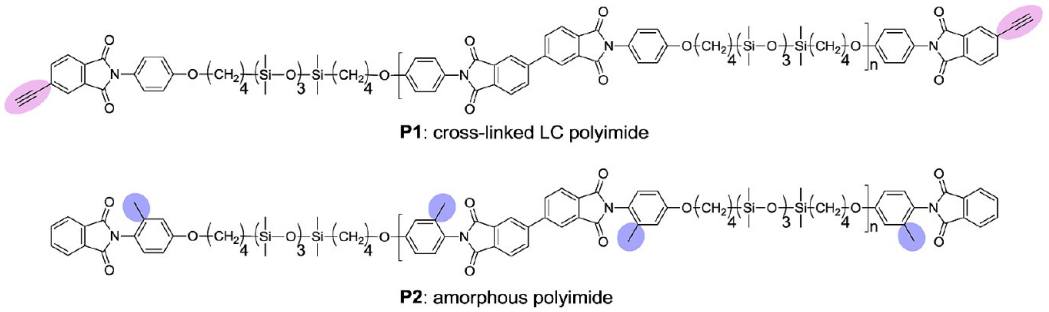

Figure 1. Cross-linked LC polyimide, **P1**, and amorphous polyimide, **P2**.

which is the medium of the thermal conduction for the organic polymers.[20]

We have previously reported the oriented cross-linked liquid crystalline (LC) polyimides with siloxane units by the cross-linking reaction of the ethynyl end-groups introduced at the chain end, increasing their thermal diffusivity in the thickness direction of the films.[21] These LC polyimides were designed toward a practical application based on a screen printing process, which included the solution processability via precursor poly(amic acid)s (PAAs) and the low phase transition temperatures derived from the flexible siloxane spacer units. It was found that the cross-linked LC polyimides formed a continuous smectic alignment from the substrate side with the increasing extent of cross-linking and this alignment gradually became disordered near the air interface side. The thermal diffusivity of the cross-linked LC polyimides in the thickness direction of the films was enhanced from 0.116 to 0.185 $mm^2\ s^{-1}$. The relationship between the chain alignments and thermal diffusivity has been clarified. However, the effect of the filler addition to the cross-linked LC polyimides has not been investigated yet.

In this work, we have developed high thermal conductive h-BN composites using the cross-linked LC polyimides as matrices, which show a vertical alignment of the smectic structures. The purpose of this work is to confirm the advantage of the oriented LC polyimide, **P1**, compared with the amorphous one, **P2**, in the composite systems (Figure 1). Indeed, the h-BN composite films of the cross-linked LC polyimide and amorphous polyimide were successfully obtained, as characterized by FT-IR spectra and SEM observation. The smectic orientation of the LC polyimide matrices was maintained even in the composites, as confirmed by wide-angle X-ray diffraction (WAXD). In the case of the cross-linked LC polyimide, the orientation of the chains did not become disordered on increasing the content of h-BN. As a result, the composites based on the cross-linked LC polyimides possess higher thermal diffusivity than the composites based on amorphous polyimides.

RESULTS AND DISCUSSION

Synthesis of Polyimide Matrices. A cross-linked LC polyimide (**P1**) and an amorphous polyimide (**P2**) with octamethyltetrasiloxane spacer units were synthesized according to a previous report by using a two-step polymerization procedure (Figure 1 and Table 1).[21−25] The chemical structures of **P1** and **P2** before cross-linking reaction were assigned by ^{1}H NMR, ^{13}C NMR, and FT-IR spectra. In addition, the results of elemental analysis agreed well with the analytical calculation values.[21] The viscosities of the resulting PAAs, which are the precursors of **P1** and **P2**, were 0.18 and 0.37 dL g^{-1}, respectively (Table 1). The number-average molecular weight and polydispersity indices (M_n; PDI) of **P1** and **P2** before the cross-linking reaction were determined to be (7,800; 2.36) and (30,500; 2.58), respectively, determined by SEC in $CHCl_3$ with calibration using polystyrene standards, as listed in Table 1. Moreover, **P1** and **P2** possessed high thermal stability over around 440 °C ($T_{d5\%}$) according to thermogravimetric analysis (TGA) under nitrogen and showed the LC and amorphous natures, respectively, as determined by differential scanning calorimetry (DSC) and polarized optical microscopy (POM) (Table 1, and see Supporting Information Figure S3).[21,24]

Table 1. Properties of Polyimide Matrices

entry	η_{inh} (dL g^{-1})[a]	M_n[b]	PDI[b]	$T_{d5\%}$ (°C)[c]	$T_{lc\text{-}cr}$ (°C)[d]	$T_{iso\text{-}lc}$ (°C)[d]
P1	0.18	7,800	2.36	448	158	192
P2	0.37	30,500	2.58	439	[e]	[e]

[a]Inherent viscosities of precursor PAAs of polyimides were measured at 30 °C in NMP at a concentration of 0.5 g dL^{-1}. [b]M_n and PDI were determined by SEC in $CHCl_3$ using polystyrene standards. [c]Decomposition temperature of the polyimide matrices. $T_{d5\%}$: 5% weight loss temperature. [d]Transition temperature of the polyimide matrices were determined as those peak tops by DSC during a cooling scan at 10 °C min^{-1}. $T_{lc\text{-}cr}$, LC-crystal transition temperature; $T_{iso\text{-}lc}$, isotropic-LC transition temperature. [e]Amorphous nature at room temperature. T_g = 76 °C, T_c = 123 °C, and T_m = 167 °C determined by the DSC trace during a heating process at 10 °C min^{-1}.

Preparation of Polyimide Composite Films. The h-BN composite solutions were prepared by mixing h-BN with the PAAs of **P1** or **P2** in *N*,*N*-dimethylacetamide (DMAc), changing the volume fraction of h-BN from 0 to 50 vol %. They were then cast and gradually heated to 200 °C on the KBr substrates to obtain the polyimide composite films. In the case of the composite films of **P1**, the cross-linking reaction and annealing treatment were carried out at 200 °C for 5 h according to the previous report,[21] whereas the composite films of **P2** were treated at 200 °C for 30 min after imidization because the lack of cross-linkers in the chain ends resulted in no cross-linking reaction from the unchanged DSC thermogram. Finally, the polyimide composite films (thickness: 125−275 μm) were successfully obtained after removal from the KBr substrates. For the characterization of the composite films, the FT-IR spectra of the composite thin films of **P1** spin-coated on a Si wafer are shown in Figure 2. The absorption band at 1381 cm^{-1}, which corresponds to the B−N stretching, is clearly observed with the increasing volume fraction of the h-BN. Moreover, the volume fraction of h-BN was estimated by calculation of the chars after TGA measurement up to 900 °C (Figure 3). Because the weight loss did not change over 700

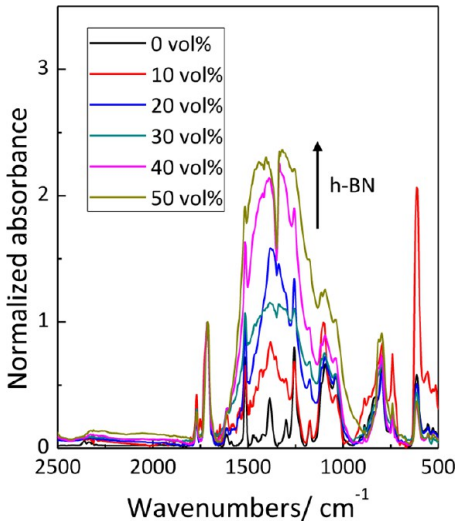

Figure 2. FT-IR spectra of the h-BN composites of **P1**.

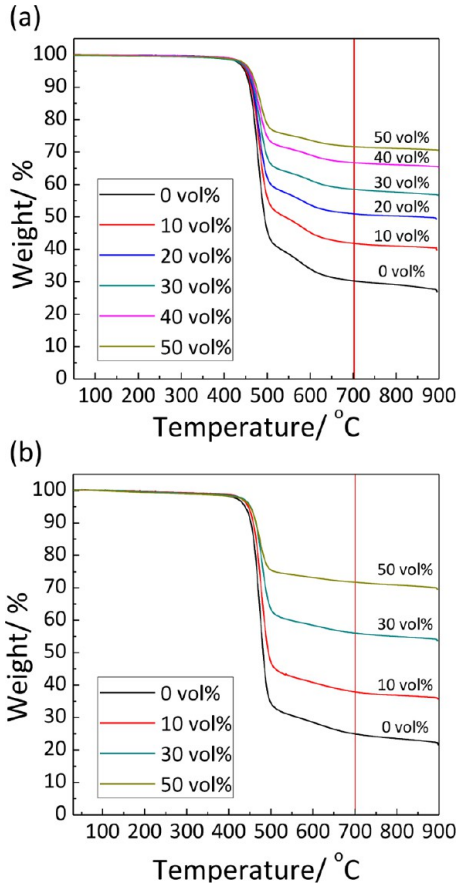

Figure 3. TGA curves of the composite films of (a) **P1** and (b) **P2**.

°C, the weight ratio values of the chars at 700 °C were estimated to determine the volume fraction of h-BN. As a result, the volume faction values were in good agreement with that of the feed values (Table 2).

Scanning Electron Microscope (SEM) Observation of the Cross-Sectional Area of Composite Films. The morphology of composite films with different h-BN contents was observed by SEM. Figures 4a–d show that the h-BN flakes are almost homogeneously dispersed through the thickness direction of the films of both polyimides **P1** and **P2** with less

Table 2. Properties of the h-BN Composite Films of the Polyimides

entry	h-BN (vol %)	h-BN (TGA) (vol %)[a]	$T_{d5\%}$ (°C)[b]	α (mm^2 s^{-1})[c]	σ (mm^2 s^{-1})[c]
P1	0	0	448	0.147	0.0230
	10	11.4	452	0.313	0.0414
	20	20.4	454	0.512	0.0690
	30	28.3	455	0.679	0.0406
	40	36.4	458	1.17[d]	0.0452[d]
	50	41.3	462	1.15[d]	0.0787[d]
P2	0	0	439	0.113	0.0038
	10	12.6	446	0.275	0.0215
	30	30.4	452	0.644	0.0291
	50	45.9	451	1.41[d]	0.0887[d]

[a]The volume fraction of h-BN was estimated by the calculation of the char weight after TGA measurement at 700 °C using the density of the graphite as a char, 2.20 g cm^{-3} and h-BN, 2.27 g cm^{-3}. [b]Decomposition temperature of the composite films. $T_{d5\%}$: 5% weight loss temperature. [c]Thermal diffusivity was measured by TWA method.[26] α: thermal diffusivity, σ: standard deviation. α shows the average value collected from 10 positions (sensor size: 0.25 mm ×0.5 mm) for the films. [d]The voids were found inside the composite films.

than 30 vol % h-BN. There is no largely aggregated h-BN in the films, although the h-BN flakes are comparatively accumulated near the KBr substrate side due to the difference in the density between h-BN and the polyimide matrices. However, a large amount of h-BN over 40 vol % leads to the production of voids inside the composite films, which appears from the KBr substrate side because of the densely dispersed h-BN at the bottom of the composite films compared to the air interface (Figure 4e). 50 vol % h-BN finally caused widely spread voids in the entire composite films (see the Supporting Information, Figure S5). The void formation was probably caused during the imidization process of the composite films, when the water molecules eliminated by the thermal dehydration of the PAAs could not come out from the composite films because of the hindrance by the large h-BN flakes.[14] For a reliable experiment, the investigation of the thermal diffusivity for the composite films was carried out using the films without any voids and with less than 30 vol % content of h-BN.

WAXD Measurements for Composite Films. In order to identify the morphology of the composite polyimides at room temperature before the thermal diffusivity measurements, WAXD measurements were performed for the composite films. The typical WAXD patterns of the composite films with different volume fractions of h-BN were obtained by the beam irradiation perpendicular to the film surface (Figure 5). The composite films of **P1** display WAXD patterns, which include a strong (001) smectic layer reflection with a *d*-spacing of 32 Å and a broad outer reflection, characteristic to the polyimide smectic LC structure reported in our previous work.[21] Besides these reflections, the (002) reflection of h-BN with a *d*-spacing of 3.3 Å appears as the most outer Debye–Scherrer ring. The WAXD patterns of the composite films of **P2** are similar to that of **P1** composite films; however, the inner reflection is not as sharp as the smectic layer reflection observed for the **P1** composite films. Besides, the **P2** composite films showed no birefringence under POM (see Figure S3 in the Supporting Information). The inner reflection could be assigned to the microsegregated layer structure (ca. 30 Å) of each component of the aromatic mesogens, the alkyl groups, and the siloxane units in the matrix **P2**.[23−25] The bulky methyl-substituent on

dx.doi.org/10.1021/am400460p | ACS Appl. Mater. Interfaces 2013, 5, 3417−3423

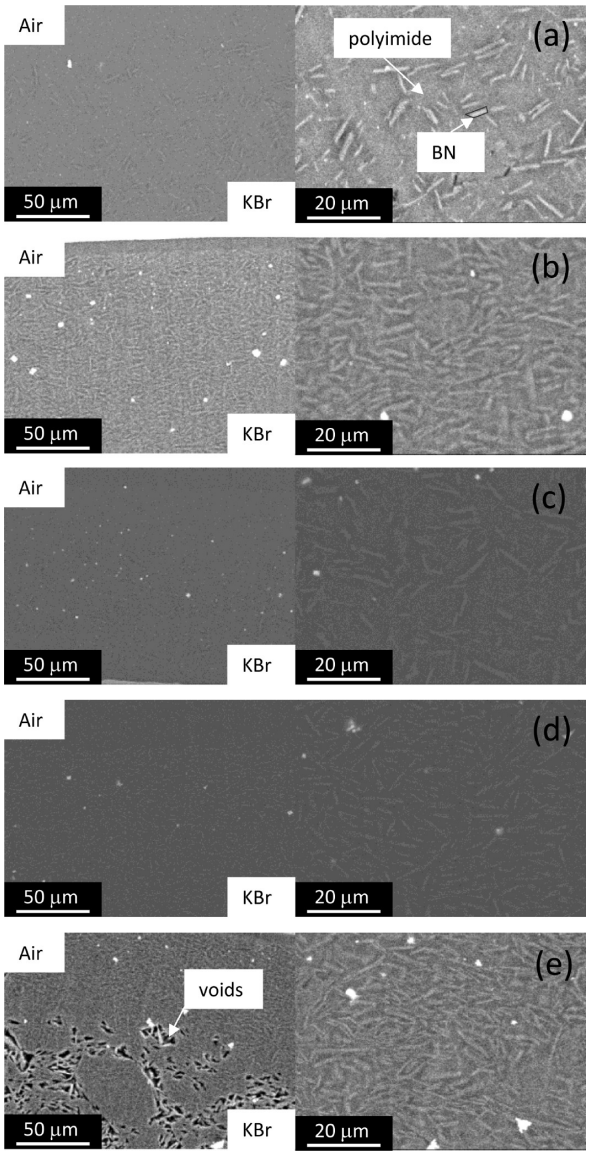

Figure 4. SEM images of the cross-sectional areas for the (a) 10, (b) 30, and (e) 40 vol % h-BN composite films of **P1**, and the (c) 10 and (d) 30 vol % h-BN composite films of **P2** (15.0 kV, × 600 (left) and ×1500 (right)). Air interface side (upper) and KBr substrate side (bottom) in each image.

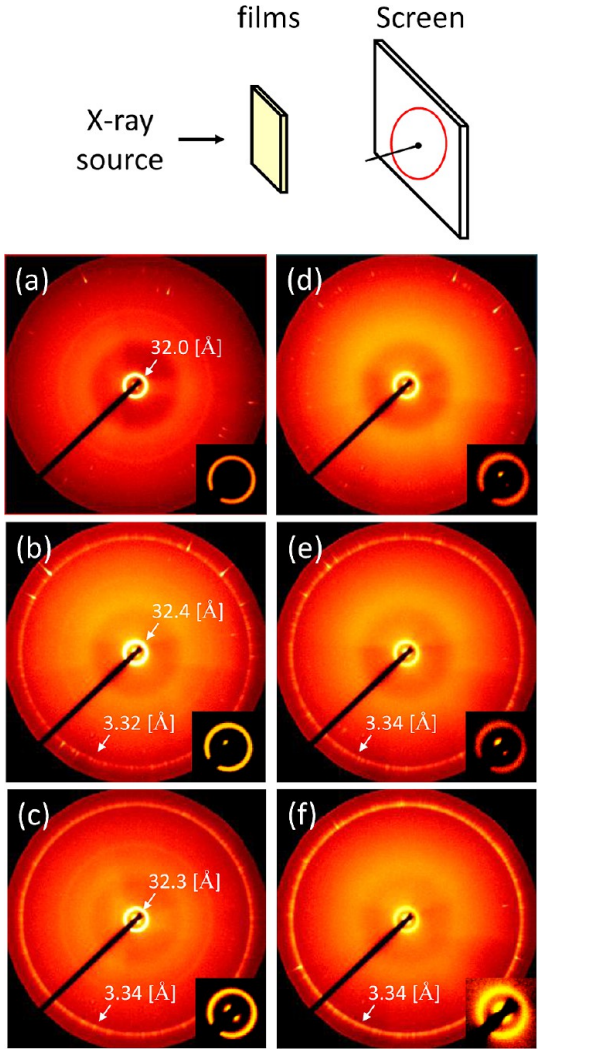

Figure 5. WAXD patterns for the (a) 0, (b) 10, and (c) 30 vol % h-BN composite films of **P1**, and the (d) 0, (e) 10 vol %, and (f) 30 vol % h-BN composite films of **P2** by the beam irradiation perpendicular to the film surface.

the mesogenic moiety may twist the imide plane to prevent the aromatic groups from forming smectic layers. Thus, the **P2** matrix is amorphous rather than liquid crystal.

While the WAXD pattern of **P1** composite films measured with beam irradiation perpendicular to the film surface includes ring-shaped reflections with isotropic intensities, that measured with beam irradiation parallel to the film surface show ring-shaped reflections with anisotropic intensities (Figure 6). The composite films of **P1**, the (001) smectic layer reflection is somewhat concentrated on the meridian, indicating that the smectic layers tend to lie parallel to the film surface, in other words, the polymer main chains align in the film normal direction.[21] Figure 7 shows the normalized intensity profiles of the (001) smectic layer in each of the diffraction patterns of the composite films of **P1** against the azimuthal angle β. It was found that the (001) smectic layer alignment in the thickness direction of the films did not become disordered even on increasing the amount of h-BN, where the orientation of the mesogenic units might be independent because the size of h-BN (around 20-μm flakes) was 3- or 4-orders larger than that of the mesogenic units. In contrast, no preferential orientation is observed for the microsegregated layer structure in the **P2** composite films (compare Figures 5d–f with Figure 6d–f). Thus, the polymer backbones of the liquid crystal **P1** matrix lie preferentially along the film normal direction, whereas that of the amorphous **P2** matrix is isotropic in the film.

On the other hand, the (002) reflection of h-BN in both series of composite films tends to concentrate on the meridian with increasing h-BN fraction (Figures 6b, c, e, and f), indicating the anisotropic dispersion of flake-shaped h-BN. There are two dimensions in the h-BN, which are the graphite-like structure with strong bonding within the planar, fused, six-membered rings (*a*-axis) and the van der Waals bonding in-between layers (*c*-axis) (see the Supporting Information, Figure S8). The SEM images of the films show that the *c*-axis of h-BN is comparatively oriented in the film thickness direction, corresponding to the anisotropic (002) reflection of h-BN in the WAXD patterns.

dx.doi.org/10.1021/am400460p | *ACS Appl. Mater. Interfaces* 2013, 5, 3417–3423

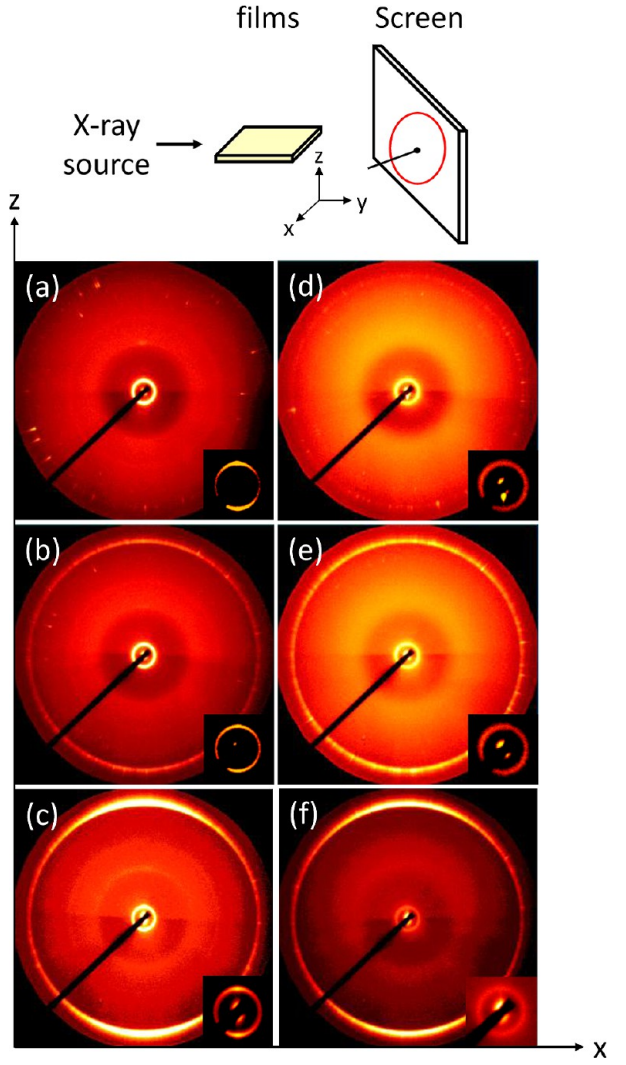

Figure 6. WAXD patterns for the (a) 0, (b) 10, and (c) 30 vol % h-BN composite films of **P1**, and the (d) 0, (e) 10, and (f) 30 vol % h-BN composite films of **P2** by the beam irradiation parallel to the film surface.

Thus, h-BN tends to align the 00*l* planes parallel to the film normal with increasing its fraction in the composite independently of the liquid crystallinity of the polyimide matrix which makes the polyimide chain backbones lie in the film thickness direction. As a result, the two types of composite films have been prepared and characterized by WAXD measurement. One is the composite film of the anisotropic polyimide matrix in the thickness direction of the film using cross-linked LC polyimides **P1**, and the other is the composite film using the amorphous polyimide matrix **P2**. The thermal diffusivity would be strongly influenced by these morphological differences in the polyimide matrices, and the anisotropic orientation could enhance the thermal diffusivity in the composite system.

Thermal Diffusivity of Composite Films. The thermal diffusivity in the thickness direction of the composite films was measured by the temperature wave analysis (TWA) method[26] at room temperature. The values of the thermal diffusivity for composite films were enhanced with the increasing volume fraction of h-BN, and the 30 vol % h-BN composite film of **P1** showed 0.679 $mm^2\ s^{-1}$, which was ca. 10% higher than that of

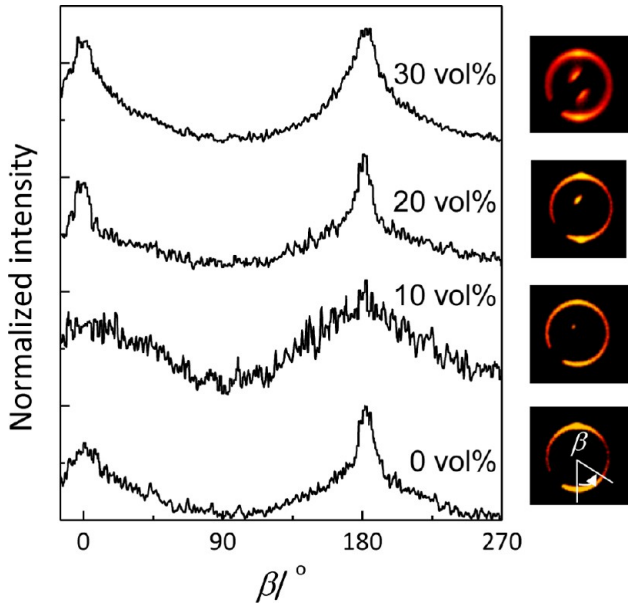

Figure 7. Normalized intensity profiles of the (001) smectic layer in each diffraction pattern for the composite films of **P1** against the azimuthal angle β.

the composite films of **P2** (Table 2 and Figure 8). As a result, the high thermal diffusivity value at the low content of h-BN in

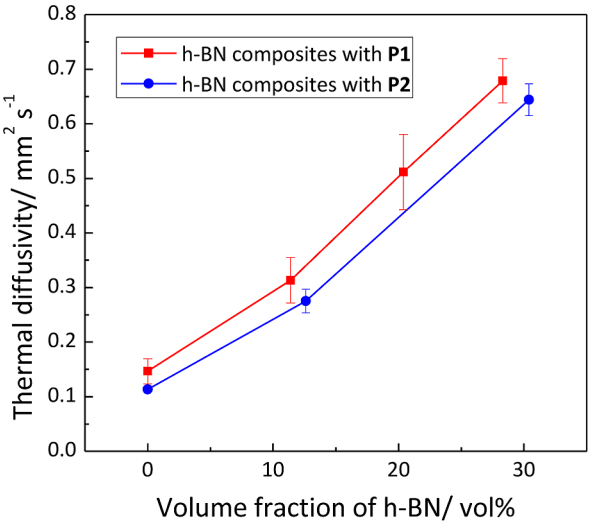

Figure 8. Plots of the thermal diffusivity in the thickness direction of the composite films at room temperature vs the volume fraction of h-BN calculated by TGA.

the composite films was successfully obtained by using the oriented polyimide matrix **P1**, approximately 5 times higher than that of the pristine film of **P1**. This result can be attributed to the homeotropic orientation of the polyimide matrix and the effective phonon conduction in the thickness direction of the films. Furthermore, the thermal diffusivity of h-BN in this work can be estimated from the equation

$$\alpha = \frac{\lambda}{\rho C_p}$$

where α is the thermal diffusivity, λ is the thermal conductivity (a-axis, 400 W m^{-1} K^{-1}; c-axis: 2 W m^{-1} K^{-1}), ρ is the density

dx.doi.org/10.1021/am400460p | ACS Appl. Mater. Interfaces 2013, 5, 3417−3423

(2.27 g cm^{-3}) and C_p is the specific heat (0.8 J g^{-1} K^{-1}).[27,28] The thermal diffusivity values of h-BN are determined to be approximately 220 mm^2 s^{-1} in the *a*-axis and 1.1 mm^2 s^{-1} in the *c*-axis, respectively. The *c*-axis of h-BN aligns in almost the same direction as the thickness one of films observed by SEM and WAXD measurements. In spite of the relatively low thermal diffusivity of h-BN in the *c*-axis compared with that in the *a*-axis, high thermal diffusivity values was obtained in the thickness direction of the films using the anisotropic polyimide matrix **P1**.

This is due not only to the existence of the *a*-axis of h-BN along the thickness direction of the films but also to the homeotropic alignment of the polymer chains serving the enhancement of the thermal diffusivity in the thickness direction of the films. Therefore, we can conclude that controlling the anisotropic orientation of the LC polyimide matrices leads to enhancing their thermal diffusivity in the oriented direction of the films when filled with h-BN. In addition, these homeotropic alignments possibly enhance not only the thermal diffusivity in the thickness direction of films but also the one parallel to the film surface.[28] However, the TWA method is difficult to apply to the thermal diffusivity parallel to the thin film. Therefore, a laser method[29] may possibly be applicable for estimating the thermal diffusivity parallel to the film surface. These measurements are in progress.

CONCLUSIONS

The h-BN composite films with high thermal diffusivity have been prepared using the cross-linked LC polyimide aligned in the thickness direction of the film as a matrix. The composite films were successfully prepared, as characterized by FT-IR, TGA, and SEM, in which the h-BN flakes were almost homogeneously dispersed in the composite films. The WAXD patterns of the composite films **P1** and **P2** obtained by beam irradiation perpendicular to the film surface corresponded to the typical smectic LC structures and the amorphous nature at room temperature, respectively. On the other hand, in the case of the results of the WAXD patterns by the beam irradiation parallel to the film surface, the layer reflections on the meridian became comparatively strong, where the smectic layer formed the vertical alignment of the polymer chains in the direction parallel to the films. Even after increasing the volume fraction of h-BN, these alignments were maintained. The thermal diffusivity in the thickness direction of the composite films was measured by the TWA method at room temperature. The thermal diffusivity values were enhanced with the increasing amount of h-BN in the anisotropic polyimide matrix **P1**, and the 30 vol % h-BN composite film of **P1** showed the highest value of 0.679 mm^2 s^{-1}. We have demonstrated the advantage of the oriented LC polyimide over the amorphous one in the composite system, showing effective phonon conduction along the oriented direction.

EXPERIMENTAL SECTION

Measurement. Inherent viscosities were measured at 30 °C in NMP at a polymer concentration of 0.5 g dL^{-1}. Number- and weight-average molecular weights (M_n and M_w) were evaluated by SEC on a HITACHI UV Dectector L-2400 equipped with a pump, an absorbance detector (UV, λ = 254 nm), and two polystyrene gel columns based on a conventional calibration curve using polystyrene standards. $CHCl_3$ (40 °C) was used as a carrier solvent at a flow rate of 1.0 mL min^{-1}. FT-IR spectra were measured on a Horiba FT-720 spectrometer. ^1H NMR spectrum was recorded with a Bruker DPX300S spectrometer. The phase transitions behavior was observed with a polarizing optical microscope (Olympus BX51), together with the use of a LINKAM LTS-350 hot stage equipped with a temperature controller by setting a polyimide film between crossed polarizers. Thermal analysis was performed on a Seiko EXSTAR 6000 TG/DTA 6300 thermal analyzer at a heating rate of 10 °C min^{-1} for thermogravimetry (TG) and a Seiko EXSTAR 6000 DSC 6200 connected to a cooling system at a heating rate of 10 °C min^{-1} for differential scanning calorimetry (DSC). To observe the cross-sectional morphology using a scanning electron microscope (SEM) with reflected electrons (FE-SEM S4500, Hitachi Ltd.), the specimens were polished by cross-section polisher with argon ion beam (SM-09020CP, JEOL Ltd.) to achieve a flat cross-section area, and then treated to carbon deposition. Wide-angle X-ray diffraction (WAXD) measurements were performed at ambient temperature by using Cu Kα radiation (50 kV, 100 mA) with a Bruker D8 DISCOVER equipped with a Vantec 500 detector. Thermal diffusivity in the thickness direction of films was measured by using ai-Phase Mobile 1u, ai-Phase Co. Ltd., based on the TWA method.[26]

Materials. Cross-linked LC and amorphous polyimides were synthesized according to the previous reports.[21−25] The h-BN filler (size: around 20 μm) was UHP-1 manufactured by Showa Denko K. K., Japan. The other materials and solvents were obtained commercially and used as received.

General Procedure for the Preparation of Composite Films. The composite films were prepared by mixing the h-BN fillers with the precursor PAAs of **P1** or **P2**. First, h-BN flakes were well dispersed in DMAc by the sonication for 3 h. Then, to a dispersed solution, the precursor PAAs were added and stirred for 24 h. The resulting PAA composite solutions were cast on KBr substrates (7 × 7 × 1 mm^3) and the obtained films were cured in the air at 200 °C. After dissolving the KBr substrate into water, the free-standing composite films were obtained with the thicknesses of 125−275 μm.

ASSOCIATED CONTENT

Supporting Information

Text giving the data for the composite films of **P1** and **P2**, which are the ^1H and ^{13}C NMR spectra of **P1** and **P2** before the cross-linking reaction (Figures S1 and S2), the DSC trace and POM images of **P1** and **P2** (Figure S3), the FT-IR spectra of the h-BN composites of **P2** (Figure S4), the SEM images of the cross-sectional area for the 20 and 50 vol % h-BN composite films of **P1**, and the 50 vol % h-BN composite film of **P2** (Figure S5), the WAXD patterns for the 20 vol % h-BN composite film of **P1** (Figure S6), the intensity profiles of the WAXD patterns by the beam irradiation perpendicular to the film surface for the 30 vol % h-BN composite films of **P1** and **P2** against 2θ (Figure S7), the schematic illustration of the h-BN lattice structure and the SEM image of the h-BN flakes (Figure S8), and the photos of the obtained h-BN composite films (Figure S9). This material is available free of charge via the Internet at http://pubs.acs.org.

AUTHOR INFORMATION

Corresponding Author

*E-mail: ueda.m.ad@m.titech.ac.jp.

Notes

The authors declare no competing financial interest.

ACKNOWLEDGMENTS

This work was supported by Grant-in-Aid for Japan Society for the Promotion of Science (JSPS) Fellows Grant (24-1018). The authors gratefully thank Mr. Jun Koki and Mr. Ryohei Kikuchi in the Department of Center for Advanced Materials Analysis, Tokyo Institute of Technology for the assistance of

SEM observation, Ms. Mizuka Tanimoto in the Department of Chemistry and Materials Science, Tokyo Institute of Technology, for providing the technical advice about the h-BN composite materials, and Ms. Chiharu Takahashi in the Department of Organic and Polymeric Materials, Tokyo Institute of Technology, for the assistance of the WAXD measurement.

REFERENCES

(1) Chung, D. D. L. *Appl. Therm. Eng.* **2001**, *21*, 1593−1605.
(2) Keith, J. M.; King, J. A.; Lenhart, K. M.; Zimmy, B. *J. Appl. Polym. Sci.* **2007**, *105*, 3309−3316.
(3) Hauaser, R. A.; King, J. A.; Pagel, R. M.; Keith, J. M. *J. Appl. Polym. Sci.* **2008**, *109*, 2145−2155.
(4) Moisala, A.; Li, Q.; Kinloch, I. A.; Windle, A. H. *Compos. Sci. Technol.* **2006**, *66*, 1285−1288.
(5) Kim, P.; Shi, L.; Majumdar, A.; McEuen, P. L. *Phys. Rev. Lett.* **2001**, *87*, 215502.
(6) Veca, L. M.; Meziani, M. J.; Wang, W.; Wang, X.; Lu, F.; Zhang, P.; Lin, Y.; Fee, R.; Connell, J. W.; Sun, Y.-P. *Adv. Mater.* **2009**, *21*, 2088−2092.
(7) Wu, H.; Drzal, L. T. *Carbon* **2012**, *50*, 1135−1145.
(8) Balandin, A. A.; Ghosh, S.; Bao, W.; Calizo, I.; Teweldebrhan, D.; Miao, F.; Lau, C. N. *Nano Lett.* **2008**, *8*, 902−907.
(9) Fukushima, H.; Drazal, L. T.; Rook, B. P.; Rich, M. J. *J. Therm. Anal. Cal.* **2006**, *85*, 235−238.
(10) Wong, C. P.; Bollampally, R. S. *J. Appl. Polym. Sci.* **1999**, *74*, 3396−3403.
(11) Zeng, J.; Fu, R.; Shen, Y.; He, H.; Song, X. *J. Appl. Polym. Sci.* **2009**, *113*, 2117−2125.
(12) Lu, X.; Xu, G. *J. Appl. Polym. Sci.* **1997**, *65*, 2733−2738.
(13) Kume, S.; Yamada, I.; Watari, K. *J. Am. Ceram. Soc.* **2009**, *92*, S153−S156.
(14) Sato, K.; Horibe, H.; Shirai, T.; Hotta, Y.; Nakano, H.; Nagai, H.; Mitsuishi, K.; Watari, K. *J. Mater. Chem.* **2010**, *20*, 2749−2752.
(15) Li, T.-L.; Hsu, S. L.-C. *J. Phys. Chem. B* **2010**, *114*, 6825−6829.
(16) Kizilkaya, C.; Mülazim, Y.; Kahraman, V.; Kayaman, N. A.; Güngör, A. *J. Appl. Polym. Sci.* **2012**, *124*, 706−712.
(17) Zhi, C.; Bando, Y.; Terao, T.; Tang, C.; Kuwahara, H.; Golberg, D. *Adv. Funct. Mater.* **2009**, *19*, 1857−1862.
(18) Song, W.-L.; Wang, P.; Cao, L.; Anderson, A.; Meziani, M. J.; Farr, A. J.; Sun, Y.-P. *Angew. Chem., Int. Ed.* **2012**, *51*, 6498−6501.
(19) Bruggeman, D. *Ann Phys* **1935**, *24*, 636−679.
(20) Akatsuka, M.; Takezawa, Y. *J. Appl. Polym. Sci.* **2003**, *89*, 2464−2467.
(21) Shoji, Y.; Ishige, R.; Higashihara, T.; Morikawa, J.; Hashimoto, T.; Takahara, A.; Watanabe, J.; Ueda, M. *Macromolecules* **2013**, *46*, 747−755.
(22) Shoji, Y.; Higashihara, T.; Watanabe, J.; Ueda, M. *Chem. Lett.* **2009**, *38*, 716−717.
(23) Shoji, Y.; Ishige, R.; Higashihara, T.; Watanabe, J.; Ueda, M. *Macromolecules* **2010**, *43*, 805−810.
(24) Shoji, Y.; Ishige, R.; Higashihara, T.; Kawauchi, S.; Watanabe, J.; Ueda, M. *Macromolecules* **2010**, *43*, 8950−8956.
(25) Ishige, R.; Shoji, Y.; Higashihara, T.; Ueda, M.; Watanabe, J. *J. Mater. Chem.* **2012**, *22*, 1532−1538.
(26) Morikawa, J.; Hashimoto, T. *J. Appl. Phys.* **2009**, *105*, 113506.
(27) Hill, R. F.; Supancic, P. H. *J. Am. Ceram. Soc.* **2002**, *85*, 851−857.
(28) Yoshihara, S.; Ezaki, T.; Nakamura, M.; Watanabe, J.; Matsumoto, K. *Macromol. Chem. Phys.* **2012**, *213*, 2213−2219.
(29) Morikawa, J.; Hayakawa, E.; Hashimoto, T.; Buividas, R.; Juodkazis, S. *Opt. Express* **2011**, *19*, 20542−20550.